

Finite resource performance of small satellite-based quantum key distribution missions

Tanvirul Islam,^{1,*} Jasmininder S. Sidhu,^{2,†} Brendon L. Higgins,^{3,‡} Thomas Brougham,²
Tom Vergoossen,⁴ Daniel K. L. Oi,² Thomas Jennewein,³ and Alexander Ling^{1,5}

¹*Centre for Quantum Technologies, National University of Singapore, 3 Science Drive 2, 117543 Singapore*

²*SUPA Department of Physics, University of Strathclyde, Glasgow, G4 0NG, UK*

³*Institute for Quantum Computing and Department of Physics and Astronomy,
University of Waterloo, Waterloo, ON N2L 3G1, Canada*

⁴*SpeQtral Pte. Ltd., 73 Science Park Drive Science Park 1, 118254 Singapore*

⁵*Department of Physics, National University of Singapore, Blk S12, 2 Science Drive 3, 117551 Singapore*

In satellite-based quantum key distribution (QKD), the number of secret bits that can be generated in a single satellite pass over the ground station is severely restricted by the pass duration and the free-space optical channel loss. High channel loss may decrease the signal-to-noise ratio due to background noise, reduce the number of generated raw key bits, and increase the quantum bit error rate (QBER), all of which have detrimental effects on the output secret key length. Under finite-size security analysis, higher QBER increases the minimum raw key length necessary for non-zero key length extraction due to less efficient reconciliation and post-processing overheads. We show that recent developments in finite key analysis allow three different small-satellite-based QKD projects CQT-Sat, UK-QUARC-ROKS, and QEYSSat to produce secret keys even under very high loss conditions, improving on estimates based on older finite key bounds.

I. INTRODUCTION

The emergence of terrestrial quantum networks in large metropolitan areas demonstrates an increasing maturity of quantum technologies. A networked infrastructure enables increased capabilities for distributed applications in delegated quantum computing [1, 2], quantum communications [3, 4], and quantum sensing [5]. However, extending these applications over global scales is currently not possible owing to exponential losses in optical fibres. Space-based segments provide a practical route to overcome this and realise global quantum networking [6]. With quantum key distribution (QKD) being a front-runner in early applications of quantum technologies, satellite-based QKD (SatQKD) has become a precursor to early applications of general quantum communications protocols [7, 8]. Although a general purpose quantum network [9] will require substantial advancements in quantum memories and routing techniques, a satellite-based QKD system adds to the progress of global-scale quantum networks by driving the maturation of space-based long-distance quantum links.

There has been growing interest in satellite-based quantum key distribution. The recent milestone achievements by the Micius satellite [10] which demonstrated space-to-ground QKD and entanglement distribution have energized this interest. Micius, being a large satellite, leaves open the possibility of using smaller satellites to perform satellite-based QKD—there have been feasibility studies for small-satellite-based QKD and CubeSat-based pathfinder missions [11] for QKD applications.

This surge in effort emphasizes the importance of understanding specific limitations to the performance of different SatQKD systems. For low-Earth orbit (LEO) satellites, a particular challenge is the limited time window to establish and maintain a quantum channel with an optical ground station (OGS). This limitation disproportionately constrains the volume of secure keys that can be generated due to a pronounced impact of statistical fluctuations in estimated parameters. These fluctuations are often ignored in applications using fibre-optical channels that can accumulate large data block sizes. Finite key analyses do not assume the availability of asymptotic data and provide a means to access performances in SatQKD.

In this work, we analyze three different mission configurations: the Singapore Centre for Quantum Technologies' CQT-Sat, the UK quantum research CubeSat/Responsive Operations for key services (QUARC/ROKS) satellite, and the Canadian quantum encryption and science satellite (QEYSSat). The quantum channel configuration for each mission is illustrated in Figure 1. In this Perspective, we revisit the supporting theory and modelling of key generation [12–16] for each of the missions to provide a realistic vision of the current progress and shed light on the most pressing challenges. We show that all three missions demonstrate enhanced key generation with the latest advancements to finite key analysis.

Depending on the ground station location and the specific LEO orbit, a satellite may have a limited number of passes over the OGS for which QKD key generation is possible—for example, current technology requires that passes are conducted during nighttime. Therefore, it is important to understand the conditions that allow a SatQKD system to produce secret keys successfully from a single pass over the OGS. More specifically, for any given satellite pass, how many secret key bits can be

* cqtmti@nus.edu.sg

† jsmdrsidhu@gmail.com

‡ brendon.higgins@uwaterloo.ca

generated? We answer this for the three mission configurations.

II. SATELLITE-TO-GROUND ENTANGLEMENT-BASED QKD USING BBM92

CQT-Sat is a 12U nano-satellite capable of performing space-to-ground entanglement-based QKD. Its precursor SpooQy-1 demonstrated [11] successful launch and operation of a miniaturized polarization entangled photon pair source in LEO. The subsequent payload will build upon this to perform space-to-ground entanglement distribution and demonstrate entanglement-based BBM92 QKD.

During a satellite's pass over the ground station, the link loss for the downlink quantum channel will depend on the relative distance between the satellite and the OGS. Using a variable attenuator, a tabletop setup can emulate a time-varying satellite-to-ground link loss (a similar experiment was conducted previously in the context of QEYSSat [17]). This enables us an estimation of the achievable raw key length and overall QBER for various satellite passes. Using these parameters we perform finite key analysis and show that CQT-Sat can successfully generate a shared secret key between the satellite and OGS when the maximum elevation is as low as 35° .

A. System configuration

The satellite quantum source generates polarization-entangled photon pairs by superposing orthogonally polarized photons created from spontaneous parametric down-conversion using two pump decay paths [18]. Detailed design of a functional model of the source and associated design trade-offs can be found in [19]. The source generates pairs of polarization-entangled photons where each pair consists of a 785 nm wavelength signal photon and an 837 nm wavelength idler photon. For the purpose of QKD, each of the idler photons is measured on-board the satellite in either the computational or the diagonal basis with probability $1/2$. The signal photon is sent to the satellite's optical terminal using an optical interface. A subsystem inside the optical source also generates a synchronization beacon. Both the beacon and the signal photons are transmitted to the OGS through the satellite's optical terminal.

Optical terminals both on the satellite and in the ground station facilitate establishing a space-to-ground free-space optical link. They consist of optical telescopes and fine pointing mechanisms for transmitting and collecting the signal photons, and synchronization and tracking beacons. Table I presents the parameters of the quantum source and the optical link.

Parameter	Value	Description
Transmitter aperture	0.09 m	Realistic aperture size for nanosatellite
Receiver aperture	0.6 m	Optimum aperture
Beam quality	1.6 M2	Fundamental limit is 1.4 due to diffraction
Atmospheric attenuation	3 dB	3 dB at zenith, scaled with path length for lower elevation
Pointing jitter	5 microrad	1.2 microrad demonstrated on Micius satellite
Efficiency	50 %	Estimated based on reflectivity and number of optical surfaces
Background counts	1300 cps	Measured with respective setup in Singapore

TABLE I. Space-to-ground optical link parameters for CQT-Sat.

B. Emulating space-to-ground QKD using a tabletop setup

To emulate a space-to-ground QKD link we built the entanglement source and the detection apparatus representative of both the satellite and ground systems. The system parameters for this setup is listed in Table II.

We consider a Sun synchronous low Earth orbit with 500 km altitude above sea level. This orbit choice gives us daily passes over our ground station at a pre-specified time of the day [20]. We compute a time series of the satellite's angular elevation with respect to the OGS and the loss at that elevation for a pass. For example, in Figure 2 we show a pass with 88° maximal elevation and associated loss that the optical link experiences.

Using a variable attenuator we introduce different losses, and record detection timestamps for both signal and idler photons. Due to physical limitations, we only use a finite number of attenuator settings, and stitch the

System Parameter	Value
Entangled pair production rate	20 Mcps
Source intrinsic QBER	0.91 %
Signal wavelength	785 nm
Idler wavelength	837 nm
Bandwidth	5 nm
Detection efficiency	25 %
Dark count rate per detector	500 cps
Detector dead time	50 ns
Detection jitter	320 ps
Detector after-pulsing probability	5 %

TABLE II. Source and detector parameters for CQT-Sat.

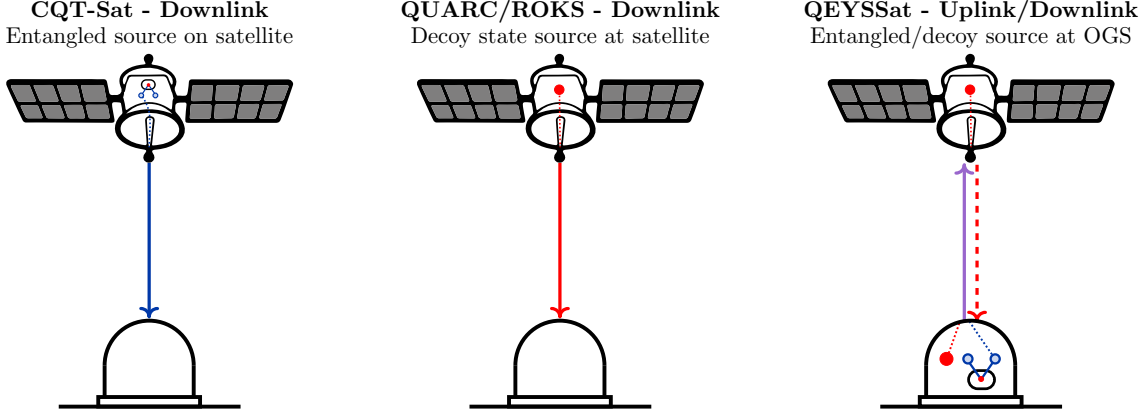


FIG. 1. Quantum channel configuration for three different SatQKD missions. Each mission implements a different combination of QKD protocols and quantum channel configurations between an OGS and an orbiting satellite. The Singaporean CQT-Sat mission (left) implements the entanglement-based BBM92 protocol (blue arrow) in a downlink configuration. For this mission, one of the photon pairs is measured on-board and the other transmitted to the OGS. The UK QUARC/ROKS mission (middle) implements the WCP decoy-state BB84 protocol (red arrow) in a downlink configuration. The Canadian QEYSSat mission (right), implements both the decoy BB84 and BBM92 protocols (purple arrow) in an uplink configuration and intends to also incorporate a decoy BB84 downlink.

experimental data together to emulate the predicted loss of the optical downlink. The blue and orange lines in Figure 2 respectively show the predicted loss and the experimentally-achieved loss at various segments of the satellite pass.

This technique allows the investigation of satellite passes with different maximum elevations and to generate the associated detection timestamps both on-board the satellite and in the OGS. These timestamp sets are processed through the rest of the QKD protocol stack including finite key analysis to compute the secure key length achievable from each pass.

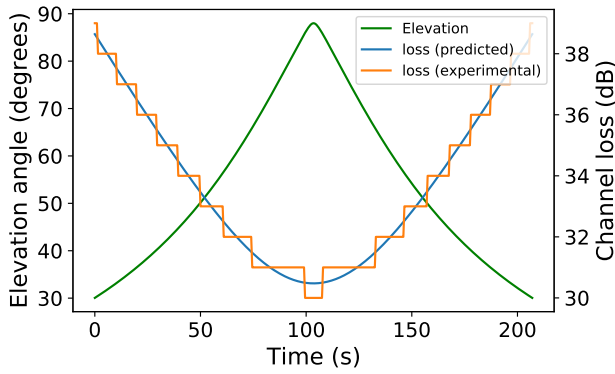


FIG. 2. Example simulated satellite pass reaching 88° elevation angle (green line). Experimental data is assembled such that its loss profile (orange line) closely matches the theoretically predicted optical loss (blue line).

C. Key length of CQT-Sat for various LEO satellite passes

Depending on geographical location and satellite orbit, a ground receiver might observe 2 to 6 satellite passes each day. An ideal satellite pass would transit directly over the ground station with maximal elevation of 90° (zenith). At zenith the satellite is closest to the OGS, and in clear weather this pass would exhibit the lowest transmission loss and longest link time. However, such a pass is less likely than more “glancing” passes. For a given detector dark count rate, higher losses would result in poorer signal-to-noise ratio and increase the QBER. Moreover, the pass duration and the number of photons successfully received from the satellite also decrease. Figure 3 shows how the secret key length changes with different satellite passes. Here we use the finite key analysis from [16] taking security parameter 10^{-10} where error correction efficiency is 1.18.

The analysis shows that below an elevation of 30° no secret key is generated. This is acceptable for CQT-Sat which was designed to avoid operation at low elevation. The ground receiver in this case is sited at sea-level in a tropical, urban environment and the optical channel below 30° is extremely lossy due to the thicker atmospheric column. Additional light pollution at low elevation is much more severe, contributing to increased noise.

III. SATELLITE-TO-GROUND QKD USING DECOY-STATE BB84

The UK Quantum Research CubeSat (QUARC) project provides a design and architectural foundation for the Responsive Operations for Key Services (ROKS) mission

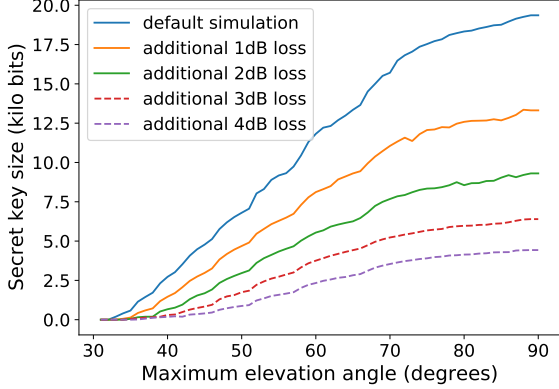


FIG. 3. Secret key length achievable for passes of given maximal elevation. The blue curve gives results for the default simulation where the minimum loss at zenith is 30.5 dB. Other curves show behaviour for optical links with additional 1 to 4 dB losses. Solid lines are based on experimental data constructed to emulate pass loss profiles. Dashed curves were simulated numerically.

in the National Space Innovation Programme (NSIP) [21, 22]. ROKS uses a continuation of the same 6U CubeSat platform as QUARC and will first implement decoy-state BB84 protocol in a downlink configuration for QKD service provision using a weak coherent pulse (WCP) source (Figure 1). The satellite quantum modelling and analysis (SatQuMA) open source software has been developed to estimate expected key generation performances for satellite QKD missions [23]. SatQuMA implements the efficient BB84 weak coherent pulse (WCP) two-decoy (three intensity) protocol and can perform optimisation over the entire protocol parameter space in addition to the transmission time window. It also incorporates recent results in finite-block composable secure key length estimation [16, 24, 25]. SatQuMA can be applied to model the expected key generation performance for ROKS for a general satellite pass geometry in a Sun-synchronous orbit (SSO) at altitude h .

A. System configuration

The Micius satellite mission published empirical measurements of the total optical loss of the SatQKD channel [26]. We use this data to construct a representative total system loss as a function of elevation angle during a satellite pass, which informs the expected detector count statistics. For any satellite pass in a SSO, we consider the portion of the pass for which the elevation is first visible above 10° , and passes below 10° to account for local horizon constraints around the OGS. The simplest type of orbit is the zenith orbit, where the satellite passes directly over the OGS.

The link efficiency is highly dependent on the system

Parameter	Value	Description
Intrinsic error	0.5%	Source errors
After-pulsing	0.1%	Probability of p_{ap}
Extraneous count rate	5×10^{-7}	Probability of counts from background light
Source rate	100 MHz	Signal frequency
Error correction	10^{-15}	Error-correction efficiency
Security	10^{-9}	Security parameter
Altitude	500 km	Satellite orbit altitude
System loss	34 dB	Loss at zenith

TABLE III. Reference system parameters. We take published information of the Micius satellite and OGS system as representing an empirically derived set point for our finite key analysis. The total loss at zenith can be linearly scaled to model other systems with smaller OGSs or differing source rates.

parameters, OGS conditions and orbits. The nominal system parameters are summarized Table III, where the minimum total system loss at zenith is computed to be 34 dB. One can scale the minimum system loss at zenith to allow the comparison of differently performing SatQKD systems. Changes to the minimum system loss at zenith would then account for differences in the transmit and receive aperture sizes, pointing accuracy, atmospheric absorption, turbulence, receiver internal losses, and detector efficiencies. For the current simulations, we consider a nominal baseline value for 34 dB. SatQKD missions with differing performance can be modelled by linearly scaling the link efficiency vs elevation curve to account for different constant efficiency factors, such as a change in OGS receiver area.

To evaluate the sensitivity of the achievable secret key length to different errors, we categorise different contributions associated with sources and detectors in two key parameters. First, errors from dark counts and background light are combined together into a single extraneous count probability p_{ec} , here assumed to be constant and independent of elevation. In practice, it will depend strongly on the environment of the OGS and light from celestial bodies. Second, all other error terms, such as misalignment, source quality, imperfect detection, are combined into an intrinsic quantum bit error rate $QBER_i$ independent of channel loss/elevation. This allows an efficient method to determine the sensitivity of the secret key length to different categories of errors, which helps identify targeted improvements for future SatQKD missions. All of the nominal system parameters are summarised in Table III.

B. Optimised finite key length

We consider the efficient BB84 protocol with signals encoded in X and Z bases with biased probabilities, and

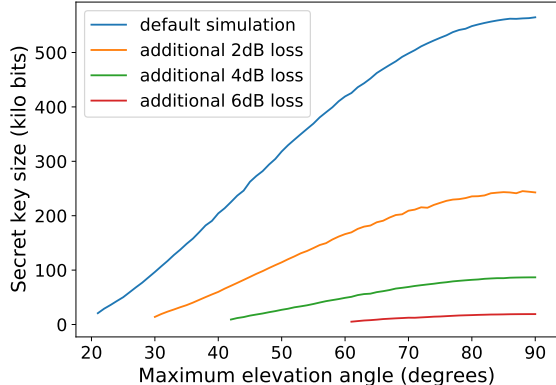


FIG. 4. Estimated secret key length generated by QUARC mission for passes with different maximum elevation angles. In the default simulation the minimum total system loss is 34 dB. Other curves show behaviour for optical links with additional 2, 4, and 6 dB losses.

adopt the convention where key generation uses the X basis and parameter estimation uses the Z basis. For a two-decoy-state WCP BB84 protocol, one of three intensities μ_j for $j \in \{1, 2, 3\}$ are transmitted with probabilities p_j . An expression for the final finite key length, ℓ , for this protocol is given in Ref. [12].

The key is constructed by processing the data for the whole pass as a single block without partitioning, possible because the security proof of Ref. [12] makes no assumptions the underlying statistics. This approach avoids having to combine small data blocks with similar statistics from different passes—thus, it is both quicker and avoids the need to track and store a combinatorially large number of link segments until each has attained a sufficiently large block size for asymptotic key extraction.

The limited data sizes from restricted pass times results in key length corrections to account for finite statistics of the link. To improve the analysis, we use the tight multiplicative Chernoff bound [15] and improve the estimate of error correction leakage $\lambda_{EC} \leq \log |\mathcal{M}|$, where \mathcal{M} characterises the set of error syndromes for reconciliation [13] (see Ref. [24] for more details).

For a defined SatQKD system, we optimise the finite key length ℓ by optimising over the protocol parameter space that includes the source intensities (with $\mu_3 = 0$) and their probabilities, and the basis encoding probability p_X . We also optimise over the portion of the pass data used for key generation. To efficiently handle this optimisation, we developed a numerical toolkit to numerically analyse different SatQKD systems. The satellite quantum modelling and analysis (SatQuMA) software assists in developing an intuition about the effects of different operational scenarios on the key rate, to better inform the development of source and receiver systems for future satellite missions [23].

The SatQuMA code is used to generate simulated mea-

surement data. The QBER and phase errors for the key bits are estimated using only the data for the complementary basis. This is a classic sampling without replacement problem, which is usually solved in QKD using an approximation for the hyper-geometric distribution [27]. Recently, however, an improved sampling bound has been proposed [16]. This can be used to estimate the QBER and phase error. The formalism from Ref. [16] is used together with data generated from SatQuMA to determine the secret key length for different satellite passes, which we characterize through the maximum elevation angle. The secret key is plotted in Figure 4 as a function of the maximum elevation angle of a pass.

IV. SATQKD USING BBM92 IN UPLINK OR DOWNLINK CONFIGURATIONS

The Quantum Encryption and Science Satellite (QEYSSat) mission [28] is a Canadian initiative to develop and launch a microsatellite-hosted quantum receiver payload into low-Earth orbit. The primary objective of the mission is to demonstrate QKD via quantum uplink from sources located at two or more ground stations. To support this, the QEYSSat payload will possess a large front-end telescope for light collection, polarization discriminating optics, and single-photon avalanche diodes [29]. Support for a WCP downlink protocol is also being developed. As of writing, QEYSSat is in the late design/early construction phase and on schedule to launch in 2023/2024.

A. System configuration

With QEYSSat’s nominal configuration being an uplink, and the quantum sources located on the ground, lower secure key rates are expected when compared to a downlink with equivalent parameters, owing to the steering effect of turbulent atmosphere on the beam at the beginning of its propagation (in contrast to the end of propagation for a downlink). However, a satellite receiver affords considerably greater source flexibility. For this reason, two source types are baselined: WCP with decoy states in an unbiased BB84 protocol, and entangled photons (with one photon of each pair kept at the ground) in a BBM92 protocol. It is expected that other quantum source types—e.g., quantum dots (see, e.g., Ref. [30])—will also be employed during the experimental phase of the QEYSSat mission.

Commencement of the QEYSSat mission in 2018 was preceded by several theoretical and experimental investigations into the mission’s feasibility, both as a whole [31] and with focus on critical subsystems including pointing [32, 33] and photon measurement [34, 35]. Of these, one early work [36] numerically modelled the quantum optical link to establish the loss and fidelity of polarized-photon transmission under the assumptions of the ex-

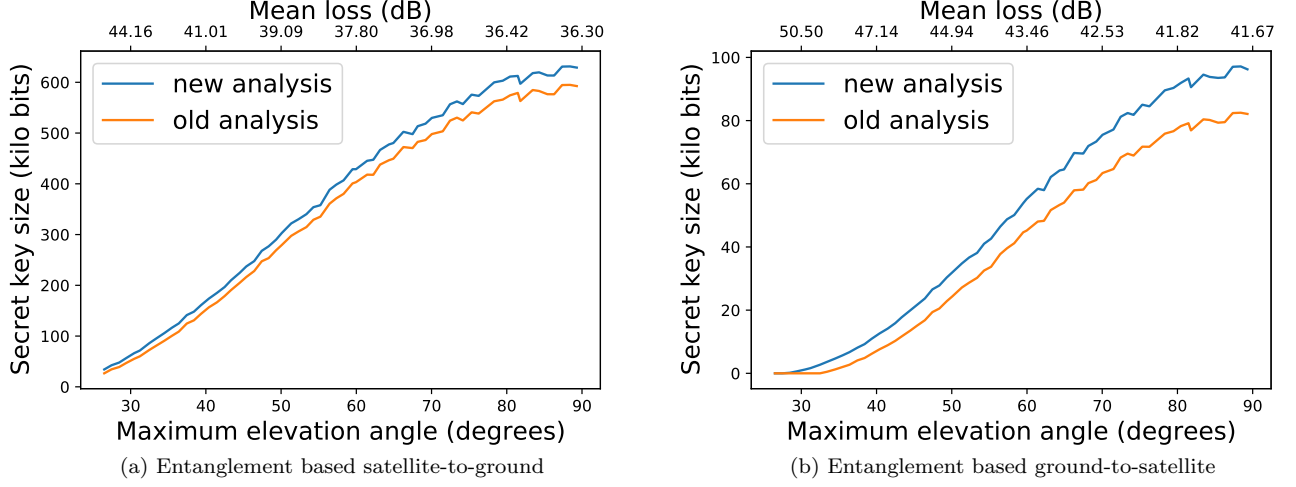


FIG. 5. Expected performance of representative conditions modelled for QEYSSat performing entanglement based QKD in (a) downlink and (b) uplink configurations. Newer finite key analysis yields improved secure key lengths.

pected orbital configuration and (generally conservative) atmospheric conditions. Multiple scenarios were considered, consisting of notional WCP or entangled-photon sources in both uplink and downlink configurations. Although some details of the in-development QEYSSat apparatus and conditions have been refined since, the values remain generally very similar. In this work we present secret key generation performance of QEYSSat while executing the entanglement-based BBM92 protocol in both satellite-to-ground (downlink) and ground-to-satellite (uplink) quantum communication configuration modes.

B. Key length analysis

In the prior analysis [36], calculations were performed using secure key rate equations which were well-established at that time—for comparison, we reproduce those calculations, with minor corrections found since publication, error correction efficiency improved to 1.18 (originally 1.22), and security parameter 10^{-9} .

More significantly, here we determine the expected secure key lengths with the same quantum transmission and fidelity profiles (corresponding to the same conditions being modeled) using updated secure key length analysis [16] which has improved performance with smaller raw key block size. Performance with smaller block size is important because it has implications on QKD feasibility under high-loss conditions and during low maximum elevation passes.

Table IV summarizes the parameters that describe the quantum source and the optical link. The assumed satellite orbit (Sun-synchronous noon/midnight at 600 km altitude) was simulated for one year’s duration of nighttime passes over a notional ground station located 20 km outside of Ottawa, Canada. Optical link conditions for

each pass were modeled at ten-second intervals. Background light was determined from the Defence Meteorological Satellite Program’s Operational Linescan System measurements and combined with an assumed half-moon at 45° (contributing via Earth reflection using its mean albedo) along with Earth’s thermal (blackbody) radiation, taking into account the geometry of the optical field of view and 1-nm-bandwidth spectral filtering. Detector dark counts were also included.

The study considered various transmitter and receiver diameters, while 50 cm and 30 cm, respectively, were baselined and will be assumed here. Optical losses were calculated from the contributions of numerically modeled diffraction given a central obstruction (secondary mirror), an assumed mean pointing error of 2 microrad, atmospheric attenuation modeled by MODTRAN 5 for a “rural” profile with 5 km visibility, and Hufnagel–Valley model of atmospheric turbulence at sea-level. Photonic

Parameter	Value
Orbital altitude	600 km
Transmitter aperture	0.5 m
Receiver aperture	0.3 m
Pointing error	2 microrad
Optics losses	3 dB
Quantum transmission wavelength	785 nm
Detector loss	2.3 dB
Spectral filtering bandwidth	1 nm
Dark count rate per detector	20 cps
EPS pair production rate	100 Mpairs/s
Source intrinsic QBER	1%
Coincidence window	0.5 s

TABLE IV. Ground-to-space optical link parameters for the model representing QEYSSat.

states were simulated in a 7-dimensional Fock-space (0 to 6 photons). Intrinsic reduction in quantum visibility was included via an operation equivalent to a small rotation.

Detector count rate statistics were calculated using assumed EPS pair production rate of 100 Mpairs/s and a 0.5 ns coincidence window. Intervals where the simulated measurement visibility was below 85% were filtered out (see Ref. [37]). For the present analysis, we aggregated the remaining statistics at each pass, and sorted these by the maximum elevation achieved by the satellite with respect to the ground station for that pass.

In Figure 5(a) and (b) we show the secret key generated for passes with different maximum elevation in the downlink and uplink configurations respectively for entanglement-based BBM92. For the new results we use the finite key analysis form from Ref. [16], with stricter security parameter 10^{-10} and error correction efficiency 1.18 to compute the secure key lengths. Notably in the uplink case, the new analysis techniques achieve almost 1/4 better key lengths for the same losses near zenith, while also accessing positive key lengths for passes with lower maximum elevations than the old analysis could tolerate (even with its more lenient 10^{-9} security parameter). We may also to compare these results with the CQT-Sat downlink scenario where finite key analysis is performed with the same parameters. Notably, the secret key size is considerably greater—we expect this is largely a consequence of the faster source rate and assumed enhancements to intrinsic QBER and pointing accuracy, coupled with the highly nonlinear effect of finite-size statistical analysis.

V. CONCLUSION

There is growing interest in deploying satellites to enable a global QKD network. To ensure that this goal is feasible, it is important to understand how satellite QKD can enable secret key generation under finite key bounds and high loss.

Previous work had shown that secret key generation from satellite QKD was possible using finite-key analysis. Recent advancements in the treatment of finite-key effects have improved the efficiency of key extrac-

tion. These latest finite key bounds have been applied to three different mission concepts; the 12U Singaporean CQT-Sat mission implementing an entanglement-based BBM92 downlink, the 6U UK QUARC project implementing a WCP decoy-state BB84 in downlink configuration, and the joint Canadian-UK QEYSSat mission implementing both the decoy BB84 and BBM92 protocols in an uplink configuration, in addition to a decoy BB84 state downlink. All three satellite QKD missions achieve a good yield of secret key material on the order of kilobits from a single pass over a ground receiver, even for the missions based on resource-constrained and aperture-limited CubeSats. This provides confidence that satellite QKD missions being planned in the next few years will yield meaningful results that can lead to an effective global QKD network.

While a rigorous comparison of the three missions is difficult owing to the operational differences, the missions have similar performances when accounting for varying source rates and the implemented protocol efficiencies.

Looking further ahead, it would be interesting to apply finite key bounds to satellite missions beyond low Earth orbit, for example to the medium Earth orbit (MEO) [38] or geostationary orbit (GEO) [39] regime. These regimes can cover a much larger surface of the Earth, but have larger diffraction losses due to the longer distances. Finite key analysis, similar to the work reported in this paper, will be one of the necessary tools employed in evaluating the cost effectiveness of satellite QKD across the different orbital regimes.

ACKNOWLEDGMENTS

J. S. S., T. B., and D. K. L. O. acknowledge support from the UK NQTP and the Quantum Technology Hub in Quantum Communications through EPSRC Grant number EP/T001011/1. B. L. H. and T. J. acknowledge support from the Canadian Space Agency, and thank J.-P. Bourgoin for discussions. T. I. and A. L. acknowledge support from the Research Centres of Excellence programme supported by the National Research Foundation (NRF) Singapore and the Ministry of Education, Singapore.

-
- [1] A. Yimsiriwattana and S. J. L. Jr., “Distributed quantum computing: a distributed shor algorithm,” in *Quantum Information and Computation II* (E. Donkor, A. R. Pirich, and H. E. Brandt, eds.), vol. 5436, pp. 360 – 372, SPIE, 2004.
 - [2] R. Van Meter and S. J. Devitt, “The path to scalable distributed quantum computing,” *Computer*, vol. 49, no. 9, pp. 31–42, 2016.
 - [3] C. Liorni, H. Kampermann, and D. Bruß, “Quantum repeaters in space,” *New J. Phys.*, vol. 23, p. 053021, may 2021.
 - [4] J. Walln fer, F. Hahn, M. G ndogan, J. S. Sidhu, F. Kr ger, N. Walk, J. Eisert, and J. Wolters, “Simulating quantum repeater strategies for multiple satellites,” *arXiv preprint arXiv:2110.15806*, 2021.
 - [5] J. S. Sidhu and P. Kok, “Geometric perspective on quantum parameter estimation,” *AVS Quantum Science*, vol. 2, p. 014701, February 2020.
 - [6] M. G ndogan, J. S. Sidhu, V. Henderson, L. Mazzarella, J. Wolters, D. K. Oi, and M. Krutzik, “Proposal for space-borne quantum memories for global quantum networking,” *npj Quantum Information*, vol. 7, p. 128, Au-

- gust 2021.
- [7] J. S. Sidhu, S. K. Joshi, M. Gündoğan, T. Brougham, D. Lowndes, L. Mazzarella, M. Krutzik, S. Mohapatra, D. Dequal, G. Vallone, P. Villoresi, A. Ling, T. Jennewein, M. Mohageg, J. G. Rarity, I. Fuentes, S. Pirandola, and D. K. L. Oi, “Advances in space quantum communications,” *IET Quantum Communication*, vol. 2, no. 4, pp. 182–217, 2021.
 - [8] A. Belenchia, M. Carlesso, Ö. Bayraktar, D. Dequal, I. Derkach, G. Gasbarri, W. Herr, Y. L. Li, M. Rademacher, J. Sidhu, D. K. Oi, S. T. Seidel, R. Kaltenbaek, C. Marquardt, H. Ulbricht, V. C. Usenko, L. Wörner, A. Xuereb, M. Paternostro, and A. Bassi, “Quantum physics in space,” *arXiv*, August 2021.
 - [9] S. Wehner, D. Elkouss, and R. Hanson, “Quantum internet: A vision for the road ahead,” *Science*, vol. 362, no. 6412, p. eaam9288, 2018.
 - [10] P. Jianwei, “Progress of the quantum experiment science satellite (QUESS) Micius project,” *Chin. J. Space Science*, vol. 38, no. 5, pp. 604–609, 2018.
 - [11] A. Villar, A. Lohrmann, X. Bai, T. Vergoossen, R. Bedington, C. Perumangatt, H. Y. Lim, T. Islam, A. Reezwana, Z. Tang, *et al.*, “Entanglement demonstration on board a nano-satellite,” *Optica*, vol. 7, no. 7, pp. 734–737, 2020.
 - [12] C. C. W. Lim, M. Curty, N. Walenta, F. Xu, and H. Zbinden, “Concise security bounds for practical decoy-state quantum key distribution,” *Phys. Rev. A*, vol. 89, p. 022307, February 2014.
 - [13] M. Tomamichel, J. Martinez-Mateo, C. Pacher, and D. Elkouss, “Fundamental finite key limits for one-way information reconciliation in quantum key distribution,” *Quant. Inf. Proc.*, vol. 16, p. 280, October 2017.
 - [14] Z. Zhang, Q. Zhao, M. Razavi, and X. Ma, “Improved key-rate bounds for practical decoy-state quantum-key-distribution systems,” *Phys. Rev. A*, vol. 95, p. 012333, January 2017.
 - [15] H.-L. Yin, M.-G. Zhou, J. Gu, Y.-M. Xie, Y.-S. Lu, and Z.-B. Chen, “Tight security bounds for decoy-state quantum key distribution,” *Sci. Rep.*, vol. 10, p. 14312, August 2020.
 - [16] C. C.-W. Lim, F. Xu, J.-W. Pan, and A. Ekert, “Security analysis of quantum key distribution with small block length and its application to quantum space communications,” *Physical Review Letters*, vol. 126, no. 10, p. 100501, 2021.
 - [17] J.-P. Bourgoin, N. Gigov, B. L. Higgins, Z. Yan, E. Meyer-Scott, A. K. Khandani, N. Lütkenhaus, and T. Jennewein, “Experimental quantum key distribution with simulated ground-to-satellite photon losses and processing limitations,” *Phys. Rev. A*, vol. 92, p. 052339, 2015.
 - [18] A. Anwar, C. Perumangatt, F. Steinlechner, T. Jennewein, and A. Ling, “Entangled photon-pair sources based on three-wave mixing in bulk crystals,” *Review of Scientific Instruments*, vol. 92, no. 4, p. 041101, 2021.
 - [19] C. Perumangatt, T. Vergoossen, A. Lohrmann, S. Sivasankaran, A. Reezwana, A. Anwar, S. Sachidananda, T. Islam, and A. Ling, “Realizing quantum nodes in space for cost-effective, global quantum communication: in-orbit results and next steps,” in *Quantum Computing, Communication, and Simulation*, vol. 11699, p. 1169904, International Society for Optics and Photonics, 2021.
 - [20] S.-K. Liao, W.-Q. Cai, W.-Y. Liu, L. Zhang, Y. Li, J.-G. Ren, J. Yin, Q. Shen, Y. Cao, Z.-P. Li, *et al.*, “Satellite-to-ground quantum key distribution,” *Nature*, vol. 549, no. 7670, pp. 43–47, 2017.
 - [21] M. Polnik, L. Mazzarella, M. Di Carlo, D. K. Oi, A. Ricciardi, and A. Arulselvan, “Scheduling of space to ground quantum key distribution,” *EPJ Quantum Technology*, vol. 7, no. 1, p. 3, 2020.
 - [22] L. Mazzarella, C. Lowe, D. Lowndes, S. K. Joshi, S. Greenland, D. McNeil, C. Mercury, M. Macdonald, J. Rarity, and D. K. L. Oi, “Quarc: Quantum research cubesat—a constellation for quantum communication,” *Cryptography*, vol. 4, no. 1, p. 7, 2020.
 - [23] J. S. Sidhu, T. Brougham, D. McArthur, R. G. Pousa, and D. K. L. Oi, “Satellite quantum modelling & analysis software version 1.1: Documentation,” *arXiv*, January 2022.
 - [24] J. S. Sidhu, T. Brougham, D. McArthur, R. G. Pousa, and D. K. L. Oi, “Finite key effects in satellite quantum key distribution,” *npj Quant. Inf.*, vol. 8, no. 1, p. 18, 2022.
 - [25] J. S. Sidhu, T. Brougham, D. McArthur, R. G. Pousa, and D. K. L. Oi, “Key generation analysis for satellite quantum key distribution,” in *Quantum Technology: Driving Commercialisation of an Enabling Science II* (M. J. Padgett, K. Bongs, A. Fedrizzi, and A. Politi, eds.), vol. 11881, pp. 1–8, International Society for Optics and Photonics, SPIE, 2021.
 - [26] J. Yin, Y.-H. Li, S.-K. Liao, M. Yang, Y. Cao, L. Zhang, J.-G. Ren, W.-Q. Cai, W.-Y. Liu, S.-L. Li, *et al.*, “Entanglement-based secure quantum cryptography over 1,120 kilometres,” *Nature*, vol. 582, no. 7813, pp. 501–505, 2020.
 - [27] C.-H. Fung, M. X., and C. H. F., “Practical issues in quantum-key-distribution postprocessing,” *Phys. Rev. A*, vol. 81, p. 012318, January 2017.
 - [28] “Quantum EncrYption and Science Satellite (QEYSSat).” <http://qeyssat.ca/>, 2022.
 - [29] A. Scott, T. Jennewein, J. Cain, I. D’Souza, B. Higgins, D. Hudson, H. Podmore, and W. Soh, “The QEYSSat mission: On-orbit demonstration of secure optical communications network technologies,” *Proc. SPIE*, vol. 11532, p. 115320H, 2020.
 - [30] P. Chaiwongkhot, S. Hosseini, A. Ahmadi, B. L. Higgins, D. Dalacu, P. Poole, R. L. Williams, M. E. Reimer, and T. Jennewein, “Enhancing secure key rates of satellite QKD using a quantum dot single-photon source,” *arXiv*, 2020.
 - [31] T. Jennewein, J.-P. Bourgoin, B. Higgins, C. Holloway, E. Meyer-Scott, C. Erven, B. Heim, Z. Yan, H. Hübel, G. Weihs, E. Choi, I. D’Souza, D. Hudson, and R. Laflamme, “QEYSSAT: a mission proposal for a quantum receiver in space,” *Proc. SPIE*, vol. 8997, p. 89970A, 2014.
 - [32] J.-P. Bourgoin, B. L. Higgins, N. Gigov, C. Holloway, C. J. Pugh, S. Kaiser, M. Cranmer, and T. Jennewein, “Free-space quantum key distribution to a moving receiver,” *Optics Express*, vol. 23, p. 33437, 2015.
 - [33] C. J. Pugh, S. Kaiser, J.-P. Bourgoin, J. Jin, N. Sultana, S. Agne, E. Anisimova, V. Makarov, E. Choi, B. L. Higgins, and T. Jennewein, “Airborne demonstration of a quantum key distribution receiver payload,” *Quantum Sci. Technol.*, vol. 2, p. 024009, 2017.

- [34] E. Anisimova, B. L. Higgins, J.-P. Bourgoin, M. Cranmer, E. Choi, D. Hudson, L. P. Piche, A. Scott, V. Makarov, and T. Jennewein, “Mitigating radiation damage of single photon detectors for space applications,” *EPJ Quantum Technol.*, vol. 4, p. 10, 2017.
- [35] I. DSouza, J.-P. Bourgoin, B. L. Higgins, J. G. Lim, R. Tannous, S. Agne, B. Moffat, V. Makarov, and T. Jennewein, “Repeated radiation damage and thermal annealing of avalanche photodiodes,” *EPJ Quantum Technol.*, vol. 8, p. 13, 2021.
- [36] J.-P. Bourgoin, E. Meyer-Scott, B. L. Higgins, B. Helou, C. Erven, H. Hübel, B. Kumar, D. Hudson, I. D’Souza, R. Girard, R. Laflamme, and T. Jennewein, “A comprehensive design and performance analysis of low earth orbit satellite quantum communication,” *New J. Phys.*, vol. 15, p. 023006, 2013.
- [37] C. Erven, B. Heim, E. Meyer-Scott, J.-P. Bourgoin, R. Laflamme, G. Weihs, and T. Jennewein, “Studying free-space transmission statistics and improving free-space quantum key distribution in the turbulent atmosphere,” *New J. Phys.*, vol. 14, p. 123018, 2012.
- [38] D. Dequal, G. Vallone, D. Bacco, S. Gaiarin, V. Luceri, G. Bianco, and P. Villoresi, “Experimental single-photon exchange along a space link of 7000 km,” *Phys. Rev. A*, vol. 93, p. 010301, Jan 2016.
- [39] B. Dirks, I. Ferrario, A. Le Pera, D. V. Finocchiaro, M. Desmons, D. de Lange, H. de Man, A. J. Meskers, J. Morits, N. M. Neumann, *et al.*, “Geoqkd: quantum key distribution from a geostationary satellite,” in *International Conference on Space Optics—ICSO 2020*, vol. 11852, p. 118520J, International Society for Optics and Photonics, 2021.